Since January 2020 Elsevier has created a COVID-19 resource centre with free information in English and Mandarin on the novel coronavirus COVID-19. The COVID-19 resource centre is hosted on Elsevier Connect, the company's public news and information website.

Journal Pre-proof

Atlas of currently-available human neutralizing antibodies against SARS-CoV-2 and escape by Omicron sub-variants BA.1/BA.1.1/BA.2/BA.3

Min Huang, Lili Wu, Anqi Zheng, Yufeng Xie, Qingwen He, Xiaoyu Rong, Pu Han, Pei Du, Pengcheng Han, Zengyuan Zhang, Runchu Zhao, Yunfei Jia, Linjie Li, Bin Bai, Ziliang Hu, Shixiong Hu, Sheng Niu, Yu Hu, Honghui Liu, Bo Liu, Kaige Cui, Weiwei Li, Xin Zhao, Kefang Liu, Jianxun Qi, Qihui Wang, George Fu Gao

PII: S1074-7613(22)00265-5

DOI: https://doi.org/10.1016/j.immuni.2022.06.005

Reference: IMMUNI 4868

To appear in: *Immunity*

Received Date: 3 April 2022

Revised Date: 13 May 2022

Accepted Date: 5 June 2022

Please cite this article as: Huang, M., Wu, L., Zheng, A., Xie, Y., He, Q., Rong, X., Han, P., Du, P., Han, P., Zhang, Z., Zhao, R., Jia, Y., Li, L., Bai, B., Hu, Z., Hu, S., Niu, S., Hu, Y., Liu, H., Liu, B., Cui, K., Li, W., Zhao, X., Liu, K., Qi, J., Wang, Q., Gao, G.F., Atlas of currently-available human neutralizing antibodies against SARS-CoV-2 and escape by Omicron sub-variants BA.1/BA.1.1/BA.2/BA.3, *Immunity* (2022), doi: https://doi.org/10.1016/j.immuni.2022.06.005.

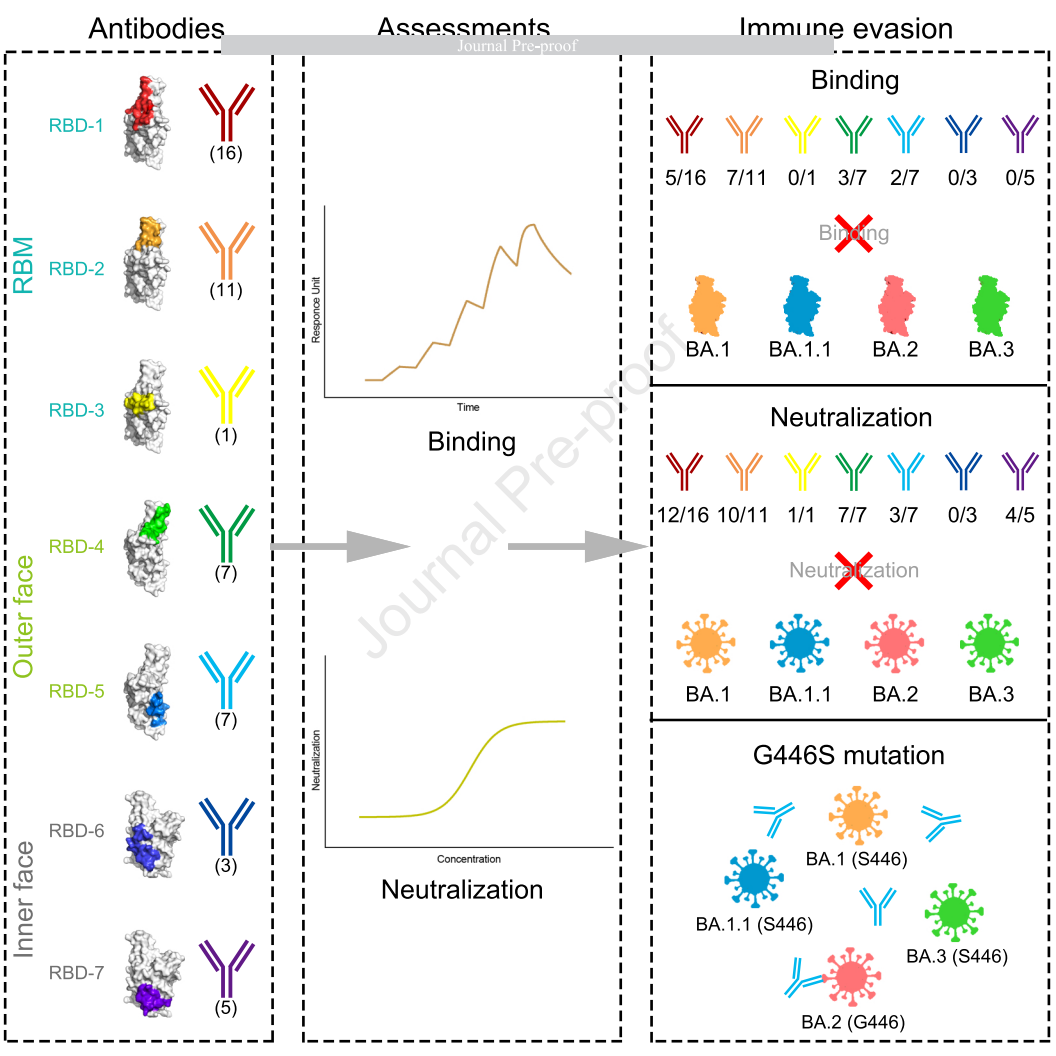

Atlas of currently-available human neutralizing antibodies against SARS-CoV-2 and escape by Omicron sub-variants BA.1/BA.1.1/BA.2/BA.3

Min Huang[1,2#], Lili Wu[2#], Anqi Zheng[2,3#], Yufeng Xie[2,4#], Qingwen He[2,5#], Xiaoyu Rong[6], Pu Han[2], Pei Du[2], Pengcheng Han[2,7], Zengyuan Zhang[2], Runchu Zhao[2,8], Yunfei Jia[2,9], Linjie Li[2,3], Bin Bai[2], Ziliang Hu[2,8], Shixiong Hu[2,9], Sheng Niu[2,9], Yu Hu[1,2], Honghui Liu[2], Bo Liu[2,9], Kaige Cui[2], Weiwei Li[2], Xin Zhao[2], Kefang Liu[2], Jianxun Qi[2*], Qihui Wang[2,3*], George Fu Gao[1,2,3,10,11*]

[1] School of Life Science, University of Science and Technology of China, Hefei, Anhui Province 230026, China

[2] CAS Key Laboratory of Pathogen Microbiology and Immunology, Institute of Microbiology, Chinese Academy of Sciences, Beijing 100101, China

[3] University of the Chinese Academy of Sciences, Beijing 100049, China

[4] Department of Basic Medical Sciences, School of Medicine, Tsinghua University, Beijing 100084, China

[5] Department of Pathogen Biology and Microbiology, Zhejiang University School of Medicine, Hangzhou, Zhejiang Province 310058, China

[6] School of Laboratory Medicine and Life Sciences, WenZhou Medical University, Wenzhou, Zhejiang, China

[7] School of Medicine, Zhongda Hospital, Southeast University, Nanjing, Jiangsu Province 210009, China

[8] Institute of Physical Science and Information, Anhui University, Hefei, Anhui Province 230039, China

[9] College of Veterinary Medicine, Shanxi Agricultural University, Jinzhong, Shanxi Province 030801, China

[10] Chinese Center for Disease Control and Prevention, Beijing 102206, China

[11] Lead Contact

[#] These authors contributed equally.

*Correspondence: jxqi@im.ac.cn (J.Q.), wangqihui@im.ac.cn (Q.W.) and gaof@im.ac.cn (G.F.G.)

SUMMARY

SARS-CoV-2 Omicron variant has presented significant challenges to current antibodies and vaccines. Herein, we systematically compared the efficacy of 50 human monoclonal antibodies (mAbs), covering the seven identified epitope classes of the SARS-CoV-2 RBD, against Omicron sub-variants BA.1, BA.1.1, BA.2 and BA.3. Binding and pseudovirus-based neutralizing assays revealed that 37 of the 50 mAbs lost neutralizing activities, while the others displayed variably decreased activities against the four Omicron sub-variants. BA.2 was found to be more sensitive to RBD-5 antibodies than the other sub-variants. Further quaternary complex structure of BA.1 RBD with three mAbs showing different neutralizing potencies against Omicron provided a basis for understanding the immune evasion of Omicron sub-variants and revealed the lack of G446S mutation accounting for the sensitivity of BA.2 to RBD-5 mAbs. Our results may guide the application of the available mAbs and facilitate the development of universal therapeutic antibodies and vaccines against COVID-19.

Keywords: SARS-CoV-2, Omicron BA.1/BA.1.1/BA.2/BA.3, human neutralizing antibodies, immune escape

INTRODUCTION

The coronavirus disease 2019 (COVID-19) pandemic, caused by severe acute respiratory syndrome coronavirus 2 (SARS-CoV-2), has been ravaging the world since the end of 2019 (Jiang et al., 2020; Tan et al., 2020; Zhu et al., 2020). In over two years, this novel coronavirus has infected over 500 million people worldwide, causing over six million deaths and great economic loss (https://covid19.who.int). In addition, SARS-CoV-2 continues to mutate and generate new variants, including Alpha, Beta, Gamma and Delta variants of concern (VOCs). A new VOC, named Omicron, with an alarmingly fast transmission rate, has recently emerged(Karim and Karim, 2021; WHO, 2021a). Confirmed cases of Omicron doubled in 1.5-3 days in areas (e.g., South Africa and the neighboring countries) with community transmission, which is significantly faster than that of Delta(Grabowski et al., 2022; WHO, 2021b). So far, Omicron has spread to all six geographic regions, surpassed Delta as the dominant VOC in many countries (https://nextstrain.org/ncov/gisaid/global), and developed several sub-lineages (e.g., BA.1, BA.1.1, BA.2, BA.3, BA.4, BA.5 and BA.2.12.1). BA.1 represented the majority of Omicron VOC until the end of 2021, at which point BA.1.1 was increasing. As of March 2022, BA.2 has surpassed BA.1 as the dominant sub-variant (WHO, 2022).

The most noticeable feature of Omicron is the surprisingly high number of mutations which are disproportionally concentrated in the spike (S) protein. BA.1 has 50 amino acid mutations in its genome, 33 of which are in the S protein. Fifteen of these are located in the receptor-binding domain (RBD) of the S protein, which is the main component included in COVID-19 vaccines, as well as the main target for neutralizing monoclonal antibodies (mAbs) (Han et al., 2022). BA.1.1 contains one more mutation (R346K) on the basis of BA.1. Additional mutations in the S protein and RBD also separate BA.2 and BA.3 from BA.1 (Figure 1). In the RBD, BA.1, BA.1.1, BA.2 and BA.3 share 12 mutations (G339D, S373P, S375P, K417N, N440K, S477N, T478K, E484A, Q493R, Q498R, N501Y, and Y505H), with one residue (S371) mutated to L371 in BA.1 and F371 in both BA.2 and BA.3. Additionally, compared with BA.1, BA.2

contains three more mutations (T376A, D405N, and R408S) but lacks G446S and G496S. BA.3 includes D405N but not G496S. Many of these mutations were rarely seen in previous VOCs (*e.g.*, G339D, S375F, and Y505H), signifying the mystery of the origins of Omicron(Du et al., 2022).

Importantly, however, some mutation sites in the RBD–such as K417, E484 and N501–are well known for causing immune escapes(Harvey et al., 2021; Li et al., 2021; Li et al., 2022; Zhou et al., 2021), while previously rare mutations represent new sites that may lead to further immune escapes. Such mutations identified in the RBD raise questions regarding the efficacy of the vaccines and antibodies currently in use against Omicron. Answers to these questions may determine the outcome of global efforts to develop herd immunity against SARS-CoV-2. Multiple reports estimate that the efficacy of some mRNA and adenoviral vector vaccines (mRNA-1273/BNT162b2 and ChAdOx1, respectively) against Omicron is significantly lower than against Delta(Hansen et al., 2021; Lopez Bernal et al., 2021; Tseng et al., 2022). A long interval between the second and third dose, with 4-6 months of ZF2001® subunit vaccine stimulates the generation of more neutralizing antibodies than those attained with a short interval (one month)(Zhao et al., 2022). The impact of Omicron mutations– that is, all mutations in sub-variant BA.1, BA.1.1, BA.2 and BA.3– on the efficacy of antibodies also requires systematic assessment, as the efficacy could be vastly diverse for different antibodies that recognize different epitopes.

A recent report categorized the current neutralizing antibodies into seven groups based on their epitopes in the RBD(Hastie et al., 2021). Antibodies in the first three groups (RBD-1, RBD-2 and RBD-3) recognize slightly different regions in the receptor-binding motif (RBM)(Wang et al., 2020). These regions are where the K417N, E484K and N501Y mutations in Alpha, Beta and Gamma VOCs that cause ineffective COVID-19 neutralizing antibodies are located. The RBD-4 and RBD-5 groups mainly contain antibodies that target the outer face of the RBD, while antibodies in groups RBD-6 and RBD-7 bind to the inner face of the RBD (Figure 1).

In this study, we selected 50 human mAbs that cover all seven groups of epitopes

in the RBD, to investigate their effectiveness against Omicron sub-variants. We assessed the binding of these antibodies to the RBDs of Omicron sub-variant BA.1, BA.1.1, BA.2 and BA.3, as well as their ability to neutralize Omicron pseudoviruses. Moreover, to reveal molecular mechanism of immune escape of Omicron, we solved the structure of a quaternary complex of Omicron BA.1 RBD with three antibodies from different groups (RBD-1, RBD-5 and RBD-7) with different neutralizing potencies. Our data demonstrate the effectiveness of a wide range of currently used SARS-CoV-2 antibodies, and may facilitate the development of universal therapeutic antibodies and vaccines to fight the ongoing COVID-19 pandemic.

RESULTS

The majority of antibodies lost binding affinity toward Omicron

To evaluate the efficacy of current human mAbs against dominant Omicron sub-variants, we first determined the binding affinities between a panel of 50 RBD-targeting neutralizing mAbs and Omicron sub-variant RBDs (BA.1, BA.1.1, BA.2 and BA.3) via surface plasmon resonance (SPR) assays with the prototype RBD and Delta RBD for comparison (Figure 1 and Table S1). According to their epitopes, these 50 mAbs (Table S1), including several in-clinical use or under development, were divided into seven groups (from RBD-1 to RBD-7) as previously defined(Hastie *et al.*, 2021). RBD-1 (16), RBD-2 (11), and RBD-3 (1) recognize the RBM, RBD-4 (7) and RBD-5 (7) bind to the outer face of RBD, while RBD-6 (3) and RBD-7 (5) recognize cryptic epitopes in the inner face of RBD.

We found that the overwhelming majority of MAbs (46/50) showed equal or enhanced binding to Delta RBD compared with those to the Prototype RBD; the exceptions were LY-CoV555 (RBD-2), BD-368-2 (RBD-4), CV07-270 (RBD-4) and C110 (RBD-5), which showed approximately 23-, 30-, 140-, and 30-fold decreases, respectively, in binding to Delta RBD (Figure 2, and Figures S1 and S2).

Of the 16 mAbs in RBD-1, five (C1A-B3, CA1-C2, C1A-F10, COVA2-04 and S2H14) completely lost the ability to bind all four Omicron sub-variant RBDs (Figure 2). Four [CB6 (LY-CoV16), B38, BD-236 and C105] retained the ability to bind BA.3 RBD but their affinities were relatively low, with equilibrium dissociation constants (K_D) > 500 nM. B38 also retained weak binding ability to BA.2 RBD, but others showed no binding to BA.2 RBD. Four (C102, CC12.1, CC12.3 and CV30) bound all four Omicron RBDs with micromolar or submicromolar affinities. Three [BD-604, BD-629 and P2C-1F11 (BRII-196)] showed nanomolar or subnanomolar binding to all four Omicron RBDs; this was particularly true of BD-604, the affinity of which was nanomolar when bound to BA.1 or BA.3 RBD (Figure 2).

Of the 11 mAbs in RBD-2, seven (LY-CoV555, Ab23, C121, C144, P2C-1A3, S2M11 and 2-4) completely failed to bind to all four Omicron sub-variant RBDs (Figure 2). COVA2-39 showed micromolar binding affinities to the four Omicron sub-variant RBDs. H4 also showed micromolar binding to BA.1 RBD but lost its binding to BA.1.1, BA.2 and BA.3 RBDs. REGN10933 and S2E12 retained relatively high binding to Omicron sub-variant RBDs with affinities ranging from 11.9 to 114.0 nM.

The single mAb in RBD-3, ADI-56046, showed relatively low binding to BA.1, BA.1.1 and BA.3 RBDs, with K_D values of 2.3 μM, 1.5 μM and 18.0 μM, respectively, and completely lost the ability to bind to BA.2 RBD (Figure 2).

Of the seven mAbs in RBD-4, five (C002, C104, P17, P2B-2F6 and S2H13) completely lost the ability to bind to four Omicron sub-variant RBDs with the exception of P17 and P2B-2F6, which bound, respectively, to BA.3 RBD and BA.2 RBD with K_D values of 3.5 μM and 5.1 μM, respectively. BD-386-2 and CV07-270 showed low binding to the four Omicron sub-variant RBDs just as P17 did to BA.3 RBD. In short, the mAbs in RBD-4 showed complete failure or relatively low abilities to bind to Omicron sub-variant RBDs.

Of the seven mAbs in RBD-5, two (C135 and 47D11) failed to bind to four Omicron RBDs. C110 and 2H04 showed micromolar or submicromolar binding to Omicron RBDs, and 2H04 lost binding to BA.1.1 RBD. REGN10987 also displayed micromolar binding to BA.1, BA.1.1 and BA.3 RBDs but showed relatively high binding to BA.2 RBD, with a K_D value of 56.7 nM as it does to Prototype RBD. C119 lost binding to BA.1, BA.1.1 and BA.3 RBDs, but showed micromolar binding to BA.2 RBD. Notably, S309–the parent antibody of sotrovimab–retained nanomolar binding affinities to four Omicron sub-variant RBDs, but displayed 2.3-14 folds decreases.

All three mAbs in RBD-6 (COVA1-16, C022 and 2-36) showed binding affinities to four Omicron sub-variant RBDs similar as those to Prototype RBD and Delta RBD. Of the five mAbs in RBD-7, H014 and S2A4 showed remarkably decreased binding, CR3022 and S304 showed similar binding, and EY6A showed moderately increased binding to Omicron RBDs compared with that to Prototype RBD and Delta RBD. Overall, most mAbs in RBD-6 and RBD-7 retained similar binding to Omicron sub-variant RBDs as to Prototype RBD, whereas mAbs in the other five groups displayed variable decreased affinities in binding to Omicron sub-variant RBDs.

The majority of antibodies lost neutralizing potency against Omicron

Based on most mAbs showing a complete loss or dramatic reduction in binding to Omicron sub-variant RBDs, we further evaluated the neutralizing activities of these 50 mAbs against four Omicron sub-variants by pseudovirus assays. As expected, in RBD-1, 12 of the 16 mAbs (CB6, B38, BD-236, C102, C105, C1A-B3, CA1-C2, C1A-F10, CC12.1, COVA2-04, CV30 and S2H14) failed to neutralize the four Omicron sub-variants, which is consistent with their failed or poor binding to Omicron sub-variant RBDs (Figure 2 and Figure S3). BD-604, BD-629, and P2C-1F11 showed partially decreased (10- to 100-fold) neutralizing abilities against Omicron sub-variants

compared to Prototype or Delta strain, with half-maximal inhibitory concentration (IC_{50}) values of < 1 μg/mL or ~1 μg/mL (Figure 2 and Figure S2). BD-604 was the most potent among the 16 RBD-1 neutralizing mAbs. CC12.3 showed a relatively weak neutralization against Omicron sub-variants, with IC_{50} values ranging from 5 to 25 μg/mL. CC12.1 completely lost inhibition to Omicron sub-variants, although CC12.1 and CC12.3 share the IGHV3-53 heavy chain(Yuan et al., 2020a). In RBD-2, 10 of 11 mAbs (REGN10933, LY-CoV555, Ab23, COVA2-39, C121, C144, P2C-1A3, H4, S2M11 and 2-4) lost the ability to neutralize the four Omicron sub-variants. The remaining mAb, S2E12, showed reduced (> 60-fold) neutralization as BD-629 in RBD-1 (Figure S2). A single mAb (ADI-56046) in RBD-3 failed to neutralize the four Omicron sub-variants due to its poor or failed bindings to Omicron sub-variant RBDs.

All seven mAbs (BD-368-2, C002, C104, COV07-270, P17, P2B-2F6 and S2H13) in RBD-4 also failed to neutralize the four Omicron sub-variants due to their poor or failed bindings to Omicron RBDs. In RBD-5, three of the seven mAbs (C119, C135 and 47D11) completely lost the ability to neutralize the four Omicron sub-variants due to their poor or failed binding. However, although REGN10987, C110 and 2H04 failed to neutralize the BA.1, BA.1.1 and BA.3 sub-variants, all of them could neutralize the BA.2 sub-variant with different potencies; this was particularly true of REGN10987, the IC_{50} of which was 0.45 μg/mL. S309 showed moderately reduced (< 10-fold) neutralization against Omicron sub-variants compared to that against the Delta and Prototype strains (Figure S2), which is consistent with the results of several recent studies(Liu et al., 2021b; Planas et al., 2021a; VanBlargan et al., 2022).

In RBD-6, all three mAbs (COVA1-16, C022 and 2-36) exhibited relatively weak neutralization against the four Omicron sub-variants; however, they showed similar binding to Omicron RBDs compared to the Prototype RBD. As previously reported(Yuan et al., 2020b), CR3022 in RBD-7 cannot neutralize SARS-CoV-2 and its variants including Delta and Omicron. H014, S2A4 and S304 lost the ability to

neutralize the Omicron sub-variants; however, EY6A showed a moderately reduced or similar ability against the Omicron sub-variants compared to that against Prototype and Delta strains. Overall, among the 50 mAbs, 36 completely failed to neutralize all four Omicron sub-variants, seven (CC12.3, P2C-1F11, C110, 2H04, COVA1-16, C022 and 2-36) showed relatively weak neutralizing abilities against 1–2 Omicron sub-variants (IC_{50} > 1 μg/mL), and others (BD-236, BD-604, BD-629, S2E12, REGN10987, S309 and EY6A) retained relatively high abilities to neutralize 1–2 Omicron sub-variants (IC_{50} <1 μg/mL) at our tested concentrations. Only BD-604 and S309 retained potent neutralizing activity against all four Omicron sub-variants, indicating remarkable immune escape of these Omicron sub-variants.

Compared with the Omicron sub-variants, these 50 mAbs showed equal or increased neutralizing activities against the Delta variant; the exceptions were BD368-2, CV07-270, C002 and C104 in RBD-4, which showed failed or remarkably deceased abilities to neutralize Delta (Figure 2 and Figure S2). As previously reported(Planas et al., 2021b), we also found that RBD-2 mAb LY-CoV555 showed a decreased neutralizing ability against Delta.

The overall structure of Omicron BA.1 RBD in complex with three mAbs targeting RBM, outer face and inner face of RBD

After screening of the 50 mAbs, we noticed that there were three mAbs, BD-604 (RBD-1, RBM), S309 (RBD-5, outer face) and S304 (RBD-7, inner face) which showed sub-nanomolar to nanomolar binding to the four Omicron RBDs but exhibited different neutralizing potencies against the four Omicron sub-variants. BD-604 and S309 partially and moderately reduced the neutralizing activity, respectively, while S304 completely abolished its potency. To understand the molecular basis of these variations, together with the mechanisms of Omicron escaping of seven groups of antibodies, we determined the quaternary complex structure of Omicron BA.1 RBD with the three mAbs at a resolution of 2.8 Å using cryo-electron microscopy (cryo-EM) (Table S2 and

Figure S4).

The overall architecture resembles the previously reported structure (PDB:7JX3) of the Prototype RBD in complex with S2H14 (RBD-1), S309, and S304 (Figure 3A)(Piccoli et al., 2020). Fifteen mutations in Omicron BA.1 RBD were displayed, of which ten (K417N, G446S, S477N, T478K, E484A, Q493R, G496S, Q498R, N501Y and Y505H) were distributed in the RBM and five (G339D, S371L, S373P, S375F and N440K) were in the outer face and inner face of the RBD (Figure 3B). Omicron S is preferentially in a state with one up-RBD or three down-RBDs, showing a more stable feature than Prototype S and Delta S (Cui et al., 2022; Hong et al., 2022). Thus, we first superimposed the quaternary complex structure onto the Omicron BA.1 S (PDB: 7QO7) in one-RBD-up conformation. This revealed that BD-604 and S309 did not clash with the adjacent RBD or NTD, whereas S304 displayed a clear steric hindrance with the adjacent RBD (Figure 3C-E).

The molecular basis of immune evasion of mAbs targeting RBM of RBD by Omicron

BD-604, as well as other antibodies in RBD-1, RBD-2, and RBD-3, recognize the RBM and generally bind up-RBD and neutralize SARS-CoV-2 infection by competition with the ACE2 receptor (Cao et al., 2020; Shi et al., 2020; Wu et al., 2020). Although BD-604 showed no clash with the adjacent protomer when binding to the S trimer, seven mutations (K417N, S477N, Q493R, Q496S, Q498R, N501Y, and Y505H) in the Omicron RBD were included in its binding epitope (Figure 3F and 4D and Table S3). Based on the reported complex structure of BD-604 binding to Prototype RBD (PDB:7CH4), we found that the binding face displayed electrostatic complementary interactions, particularly the positively charged bulge on Prototype RBD formed by K417, which inserted into the negatively charged groove formed by the heavy chain (H) and light chain (L) of BD-604 (circle a, Figure 4A and 4B). However, the K417N mutation reduced the positively charged features of the Omicron RBD (Figure 4C). In

addition, although T478 is not included in the epitope of BD-604, K478, with a positive charge, strengthened the electrostatic repulsion between RBD and the H chain of the antibody (circle b). These factors led to BD-604 binding to Omicron RBD with approximately a 3 Å shift compared to that bound to Prototype RBD (Figure 4D), and this may also be enhanced by Q493R and Q498R mutations due to the longer side chain of arginine. Furthermore, we found that five hydrogen bonds (H-bonds) between the H chain of BD-604 and RBD were broken, which were contributed by G26 (HCDR1) with N487, S53 (HCDR2) with Y421, S53 with R457, and R97 (HCDR3) with Y489 (Figure 4E and 4F, and Table S6), and three H-bonds between the L chain and RBD were broken, which were formed by Q27 (LCDR1) with G502, G28 (LCDR1) with G502, and N92 (LCDR3) with R403 (Figure 4G and 4H, and Table S6). The Q493R and Q498R mutations resulted in the loss of four H-bonds formed by Y102 (HCDR3) with Q493, S30 (LCDR1) with Q498, and S67 (LCDR2) with Q498 (Figure 4E-H). BD-604 completely and partially lost the van der Waals interaction with S496 and N477 compared to that with G496 and S477 (Table S3). However, N501Y and Y505H mutations enhanced the interaction with BD-604 (Figure 4G and 4H, and Table S3). Moreover, the L chain of BD-604 formed two new salt bridges with Omicron RBD by the interaction of D32 with R493 and D94 with R408 (Figure 4G and 4H, and Table S6). Although BD-604 maintained considerable interaction with Omicron, its binding was lower than that to Prototype RBD because of the seven mutations included in its epitope (Figure 3F). These results could explain why BD-604 exhibited reduced neutralization ability against Omicron (Figure 2). We confirmed that the decrease in the neutralization of most antibodies recognized RBM (RBD-1, RBD-2 and RBD-3) was caused by residue mutations, including used LY-CoV16 (CB6), LY-CoV-555 and REGN10933. For representative CB6, the K417N mutation broke the salt bridge interaction with D104 in the H chain, and the Q493R mutation displayed steric hindrance with Y102 in the H chain because of the longer side chain of R (Figure 4I). These results led to CB6 losing the binding and neutralizing abilities to the four Omicron sub-variants because all of them bear K417N and Q493R mutations. In

addition, for CC12.1 and CC12.3, the H chains–which use the same germline gene (IGHV3-53)–four mutations (K417N, S477N, E484A, and Q493R) carried by all four Omicron sub-variants led to the loss of many interactions with CC12.1, including those containing salt bridges, H-bonds, and van der Waals interactions, as well as the addition of a steric clash that resulted in the failed neutralization of CC12.1 against the Omicron sub-variants (Figure 4J). However, just two mutations K417N and Q493R affected its interaction with CC12.3 (Figure 4K). Thus, these results could explain why CC12.3 shows slightly better binding and neutralization to Omicron than CC12.1 (Figure 2).

The molecular basis of immune evasion of mAbs targeting outer face of RBD by Omicron

S309, as well as other mAbs in RBD-5 and RBD-4, recognize the outer face of the RBD, bind both up-RBD and down-RBD within the S trimer, and potently neutralize SARS-CoV-2 by cross-linking spike proteins (Pinto et al., 2020). Compared to the previous report of the structure of S309 in complex with Prototype RBD (PDB: 7JX3), we found that S309 bound to Omicron RBD was similar to that bound to Prototype RBD, with a ~1.8 Å shift (Figure 5A, and Tables S6); two mutations in Omicron, G339D and N440K, contributed to the interaction with S309 (Figure 4F and 5A). The G339D mutation resulted in the loss of two H-bonds formed by the interaction of Y100 (HCDR3) with G339 and A104 (HCDR3) with E340 (Figure 5B and Table S4). However, the N440K mutation introduced one van der Waals contact with S31 (LCDR1) (Figure 5B). Moreover, glycosylation of RBD N343 contributed to many interactions for the binding of S309 to RBD. In the previous structure, N343 was glycosylated with one N-acetylglucosamine (NAG), which contributed six van der Waals contacts to bind to Y100 (HCDR3) and Y50 (LCDR2) (Figure 5C, right panel). In our structure, the glycosylation of N343 was heavier with two NAGs and one fucose, (FUC), and formed more interactions with S309 than that in Prototype RBD (Figure 5C, left panel). These results could explain why S309 showed only moderately reduced binding and neutralization ability against the three Omicron sub-variants (Figure 2). However, other

antibodies in RBD-5 and RBD-4 showed reduced neutralization against Omicron (Figure 2). For example, REGN10987, the epitope of which is closer to RBM than S309, and the binding is mainly affected by G446S and N440K mutations (Figure 5G). The G446S mutation breaks the hydrophobic patch contributed by V445, G446, G447, and Y449 in the RBD and V50, I51, Y53, G55, Y59, and Y105 in the H chain, and displays steric clash with N57 in the H chain. The N440K mutation also displays a potential clash with Y102 in the H chain. These results suggest that REGN10987 fails to bind and neutralize BA.1, BA.1.1 and BA.3, all of which carry N440K and G446S mutations, whereas the mAb retains binding and neutralization against BA.2, owing to the lack of the G446S mutation.

G446S mutation impaired the efficacy of RBD-5 mAbs against Omicron

To confirm our hypothesis that G446S mutation impaired the efficacies of RBD-5 mAbs, we further assessed the binding affinities of RBD-5 mAbs to BA.2 RBD with G446S by SPR assays. As expected, REGN10987, C110 and C119 showed decreased binding to BA.2 RBD with G446S mutation compared to those to BA.2 RBD (Figure 6). C135 and 47D11 displayed no binding to BA.2 RBD with G446S as to BA.2 RBD. While S309 and 2H04 showed similar binding to BA.2 RBD with or without G446S, since this site is beyond their epitopes. However, the binding abilities of 2H04 to both RBDs are much lower than S309. Then, we evaluated the neutralizing potencies of these RBD-5 mAbs against BA.2 pseudovirus with G446S. We found that REGN10987, C110 and 2H04 completely lost neutralization, and C119, C135 and 47D11 showed no neutralization, against BA.2 pseudovirus with G446S (Figure 2). In contrast, S309 displayed similar neutralizing abilities against BA.2 pseudoviruses with or without G446S. These results were consistent with the SPR data. Additionally, the data indicated that the neutralizing activities of the mAbs in the other six groups were not affected by G446S mutation (Figure 2), which further supports our hypothesis.

The molecular basis of immune evasion of mAbs targeting inner face of RBD by

Omicron

S304 and other antibodies in RBD-7 and RBD-6 recognize cryptic epitopes at the interface of RBD, require at least two RBDs in an up-conformation for binding to the S trimer, and neutralize SARS-CoV-2 by partially clashing with ACE2 or cross-linking spike proteins (Piccoli *et al.*, 2020). In comparison with previously reported structures(Piccoli *et al.*, 2020), we found that although no mutation in Omicron RBD was included in the binding face, the epitope of S304 was close to the S371L, S373P, and S375F mutations, which drives a conformational shift of the α2βc2 loop (Figure 4F and 5D, Table S5). This shift destroyed the interaction of N370 with G55 and T57 in the H chain of S304 (Figure 5E and Table S5). Although S304 retained a relatively strong interaction with Omicron RBD compared to that with Prototype RBD (Figure 5E and 5F and Table S5), it was ineffective in neutralizing Omicron because of the preferential conformation of Omicron S in the one-RBD-up conformation. Similarly, the other mAbs in RBD-6 and RBD-7 also showed weak neutralization ability against the Omicron variant, although their binding to Omicron RBD was equal to that to Prototype RBD and Delta RBD, except for H014, S2A4, and EY6A. H014 and S2A4 exhibited reduced binding and failed neutralization to Omicron. In contrast, EY6A showed slightly increased (approximately 3-fold) binding and decreased (approximately 5-fold) neutralization to Omicron (Figure 2). For S2A4, the S371L and S375F mutations break the H-bond interaction with R103 in the H chain and N32 in the L chain, respectively (Figure 5H). The S373P mutation and the shift of the α2βc2 loop may increase the steric clash with the L chain. These two mutations also affect the binding of H014 to Omicron. These results lead to S2A4 and H014 showing relatively weak binding and disabled neutralization to Omicron sub-variants. Based on the reported structure of EY6A in complex with Prototype RBD (PBD: 6ZCZ) or Omicron RBD (PDB: 7QNW)(Dejnirattisai et al., 2022), we found that S373P and S375F mutations enhanced H-bond interactions with K65 in the H chain (Figure 5I). In addition, S373P also increased the hydrophobic interaction with Y60, V64, G66, and F68 in the H chain (Figure 5I). These results could explain why EY6A enhanced

binding to Omicron RBD (Figure 2). Taken together, EY6A still showed reduced neutralization against Omicron sub-variants due to the preferential conformation of Omicron S in one-RBD-up conformation.

L452R mutation impaired the efficacy of RBD-4 mAbs against Delta

Compared to the four Omicron sub-variants, Delta carries a unique L452R mutation on RBD. Though the L452R is located in the RBM region, it does not directly participate in the interaction with ACE2 receptor(Han *et al.*, 2022; Wang *et al.*, 2020). However, as several studies reported, L452R mutation could reduce the sensitivity to mAbs and sera elicited by vaccines or infections based on the prototype SARS-CoV-2, which increases the immune escape of Delta(Liu et al., 2021a; Planas *et al.*, 2021b). In our study, we found Delta particularly escaped RBD-4 mAbs due to the L452R mutation. As exemplified by BD-368-2, L452R mutation broke the hydrophobic interaction formed by G26, F27, A28, F29, Y32 and A33 on heavy chain of the mAb and Y449, Y451, Y453 and L455 on RBD, and increased potential clash with T31 on heavy chain (Figure S5). Consequently, BD-368-2 showed 30-fold decreased binding to Delta RBD and failed neutralization against this variant (Figure 2).

DISCUSSION

Studies suggest that the Omicron BA.1 sub-variant is resistant to the majority of antibodies currently used against COVID-19. However, owing to the increasing prevalence of other sub-variants in many countries, the potential immune evasion of BA.1.1, BA.2 and BA.3 sub-variants needs to be clarified immediately. Herein, we selected 50 human neutralizing mAbs, recognizing seven classes of epitopes in the RBD, to compare immune evasions of BA.1, BA.1.1, BA.2 and BA.3 sub-variants. As expected, we found that BA.1.1, BA.2 and BA.3 showed immune escapes as remarkable as that of BA.1, indicating that these four sub-variants have similar evasion spectra. We noted, in particular, that BA.2 was more sensitive to RBD-5 antibodies than BA.1 BA.1.1 and BA.3, owing to the lack of G446S mutation. As exemplified by RBD-

5 mAb REGN10987, G446S was crucial to impairing the binding of the antibody, destroying the strong hydrophobic patch formed by V445, G446, G447, and Y449 in the RBD and several hydrophobic residues in the antibody. As BA.2 has no G446S mutation, it retains some sensitivity to REGN10987. Our data further suggested that G446S impaired the efficacies of RBD-5 mAbs by SPR and neutralization experiments. Additionally, the effect of G446S mutation was also confirmed by a recent study which found that this single mutation can impair the neutralizing ability of REGN10987 by more than 500-fold compared to the antibody against SARS-CoV-2 prototype pseudovirus (Liu *et al.*, 2021b). Similarly, C110 and 2H04 also showed a little bit neutralizing ability against BA.2, but not BA.1 and BA.3, which include G446S.

Although some representative antibodies in RBD-6 and RBD-7 can bind BA.1, BA.1.1, BA.2 and BA.3 RBDs well, most of them showed weak or ineffective neutralization against these four sub-variants, which was consistent with the dominant state of Omicron S in the one-RBD-up conformation as these two classes of antibodies recognize cryptic epitopes and require at least two RBDs in the up state. Free Omicron S proteins in two-RBD-up, and three-RBD-down conformation have also been observed(Gobeil et al., 2022), and the complex structure of Omicron S in the two-RBD-up conformation bound to two ACE2s has been reported(Cui *et al.*, 2022; Hong *et al.*, 2022), indicating the limited conformational shift of Omicron S proteins and providing the structural basis to explain why RBD-6 and RBD-7 antibodies show certain neutralizing abilities against Omicron, although Omicron S proteins are preferentially in the one-RBD-up conformation. These results suggest that apart from the residue substitutions, the conformational shift of the S protein is also an important factor for immune evasion. However, many questions regarding the conformation of Omicron S still need to be answered. For example, further studies are required to clarify if the binding of ACE2 or an antibody to one RBD could induce a conformational change of the adjacent RBD.

The current strategies grouping COVID-19 antibodies are based on their epitope landscapes on SARS-CoV-2 prototype RBD. However, with the emergence of Omicron, several reports as well as our study found that most antibodies exhibited completely or partially lost efficacies and few retained potencies against this variant, even if they belonged to the same epitope cluster. Therefore, new strategies for RBD groupings might be needed for Omicron. Here, we re-evaluated and classified these 50 mAbs into three groups according to them with or without Omicron binding (Figure S6A). Group 1 (G1) indicates the mAbs that can bind to the Omicron RBD, and also confer neutralizing activities against Omicron sub-variants. This group contains 13 members, most of which belong to RBD-1, RBD-5 and RBD-6 in the Hastie's system (Hastie *et al.*, 2021). Group 2 (G2) indicates the mAbs that can bind to the Omicron RBD, but not neutralize Omicron VOC. This group includes 20 members, most of which belong to RBD-1, RBD-3, RBD-4 and RBD-7. Group 3 (G3) indicates the mAbs neither bind nor neutralize Omicron, containing 17 members, which mainly fall into RBD-1, RBD-2 and RBD-4 communities. These results imply the diversity of RBD-1 mAbs, due to their distribution of all three new identified groups. Notably, among these 50 mAbs, there are three superior mAbs (IC50 < 1 μg/mL) for Omicron, BD-604, S2E12 and S309, belong to RBD-1, RBD-2 and RBD-5, respectively (Figure S6B). However, these are three individual cases. Further studies are needed to determine the neutralizing activities of mAbs against Omicron variants targeting these epitopes.

New variants and sublineages may continue to emerge in the future. With such high transmission levels, SARS-CoV-2 has abundant opportunity to reproduce and for errors or mutations to continue to arise. The way to address this issue is to try to slow transmission and reduce the pool of susceptible hosts in which the virus can freely replicate. Strategies such as social distancing and mask-wearing, as well as increasing global vaccination rates, will slow the emergence of new variants and lineages. Additionally, broad-spectrum vaccines and therapeutic antibodies are urgently needed to fight COVID-19. Antibodies such as BD-604 and S309, especially S309, which can

recognize both up-RBD and down-RBD, should be the focus of future therapeutic development. Researchers should also enhance the stability of epitopes of these antibodies when designing vaccines. In addition, further studies to develop antibodies or peptides targeting the conserved S2 region of S proteins and small therapeutics targeting conserved polymerase or protease of SARS-CoV-2 are required to overcome the current Omicron sub-variants and future potential variants.

LIMITATIONS OF THE STUDY

There are some limitations to the interpretation of this study. First, during the revision, new Omicron sub-variants (e.g., BA.4, BA.5 and BA.2.12.1) are emerging with different mutations and fast transmission, drawing public's attention and concern. Thus, their immune evasion features should be investigated in the further study. Second, this study included 1 and 3 mAbs in RBD-3 and RBD-6 community, respectively, due to limited availability of RBD-3 and RBD-6 when we set up the experiments. However, more mAbs are being reported and more members in the two communities should be evaluated in the further study for more accurate characterization of the immune evasion of Omicron sub-variants. Third, new neutralizing epitope of RBD has been identified, with the addition of the seven communities, thus, their neutralizing activities against Omicron sub-variants need further study.

ACKNOWLEDGEMENTS

We are grateful to Z. Fan (Institute of Microbiology, Chinese Academy of Sciences [CAS]) and Z. Yang (Tsinghua University) for their technical support of SPR analysis. We thank Novoprotein Scientific Inc. for their support on Omicron RBD expression. This work was supported by the CAS Project for Young Scientists in Basic Research (YSBR-010), the National Natural Science Foundation of China (81922044, 82041047 and 81973228) and the Strategic Priority Research Program of the Chinese Academy of Sciences (XDB29040203). L.W. is supported by the China Postdoctoral Science Foundation (2021M703446). Q.W. is supported by the Youth Innovation Promotion

Association CAS (2018119).

AUTHOR CONTRIBUTIONS

Q.W. and G.F.G initiated and coordinated the project. Q.W. designed the experiments. M.H. and Q.H. performed the SPR analysis. A. Z. and M.H. performed the pseudovirus neutralization assay. M.H. prepared the proteins of Omicron BA.1 RBD in complex with BD-604, S309, and S304. Y.X. collected the structural data and solved the cryo-EM structure. L.W., M.H., A.Z., Q.W. and G.F.G analyzed the data. L.W., P.D., M.H., Q.W. and G.F.G wrote the manuscript.

DECLARATION OF INTERESTS

The authors declare no competing interests.

529 **Figure legends**

530 **Figure 1. Amino acid mutation mapping of RBDs from SARS-CoV-2 Prototype**
531 **and VOCs.** Three major epitopes on SARS-CoV-2 RBD targeted by seven classes of
532 mAbs (RBD-1 to RBD-7), and residue mutation mapping of RBDs from SARS-CoV-2
533 VOCs. See also Table S1.

534

535 **Figure 2. Binding and neutralizing abilities of current antibodies to Omicron BA.1,**
536 **BA.1.1, BA.2 and BA.3 sub-variants**. 50 mAbs were divided into seven groups (RBD-
537 1 to RBD-7) shown in different colors. The indicated antibodies in the supernatant were
538 captured by a Protein A chip. Then, serially diluted Omicron RBD, Delta RBD, and
539 Prototype RBD were flowed over the chip surface to assess binding to the indicated
540 antibodies, respectively. The binding affinity (K_D) of each pair of interaction are shown
541 as mean ± SD of three independent experiments. SARS-CoV-2 Omicron, Delta, and
542 Prototype pseudoviruses were incubated with four-fold serial dilutions of antibodies,
543 respectively. Then, the mixtures were added to Vero cells. After 15 h, the infected cells
544 were counted with a CQ1 Confocal Quantitative Image Cytometer. The experiments
545 were performed at least twice with two replicates (n = 2), and the IC_{50} values are one
546 representative data of two independent experiments. PT indicates prototype SARS-
547 CoV-2. See also Figures 1-3.

548

549 **Figure 3. Overall structure and epitope comparison of BD-604, S309 and S304**
550 **binding to Omicron BA.1 RBD. A** Overall structure of BD-604, S309 and S304
551 binding to Omicron BA.1 RBD. All structures are shown in cartoon with different
552 colors. **B** The footprints of BD-604, S309 and S304 in Omicron BA.1 RBD shown in
553 magenta, green and yellow, respectively. 15 mutations in BA.1 RBD are shown in
554 purple color. The RBM region is circled in blue dotted line. **C-E** The side (**C** and **D**)
555 and top (**E**) views of BD-604, S309 and S304 binding to BA.1 S trimer in one-RBD-up
556 conformation. The BA.1 RBD/BD-604/S309/S304 complex was superimposed onto the
557 BA.1 S trimer (PDB: 7QO7). S trimer is shown in gray color. **F** The sequence alignment

of RBDs of Omicron BA.1, BA.2 and BA.3, generated by ESPript 3.0. The binding sites of BD-604, S309 and S304 in BA.1 RBD and Prototype RBD are indicated in triangles with different colors. See also Figure S4; Tables S2-S5.

Figure 4. Structural details of immune evasion of BD-604 and related antibodies by Omicron sub-variants.

A Electrostatic surface view of BD-604. **B** Electrostatic surface view of Prototype RBD. **C** Electrostatic surface view of Omicron BA.1 RBD. **D** The overall comparison of two complex structures of BD-604/Prototype RBD and BD-604/BA.1 RBD by aligning the two RBDs. BD-604/Prototype RBD complex was shown in gray ribbon, and BD-604/BA.1 RBD was shown in corresponding color as in Figure 4. Mutant residues in BA.1 RBD contributed interaction with BD-604 were shown in sphere. **E-F** The detailed interaction between H chain of BD-604 and the BA.1 RBD (**E**) or Prototype RBD (**F**). The residues involved in the interaction were labeled, and H-bonds were shown as dotted lines with a cutoff of 3.5 Å. **G-H** The detailed interaction between L chain of BD-604 and the BA.1 RBD (**G**) or Prototype RBD (**H**). The residues involved in the interaction were labeled, and H-bonds were shown as dotted lines with a cutoff of 3.5 Å. **I-K** Binding face between RBD and representative mAbs, including CB6 (**I**), CC12.1 (**J**), and CC12.3 (**K**). All structures were shown in cartoon with the key residues in stick. H-bonds were shown as dotted lines with a cutoff of 3.5 Å. See also Tables S3 and S6.

Figure 5. Structural details of immune evasion of S309, S304, and related antibodies by Omicron sub-variants.

A The overall comparison of two complex structures of S309/Prototype RBD and S309/BA.1 RBD by aligning the two RBDs. S309/Prototype RBD complex was shown in gray ribbon, and S309/BA.1 RBD was shown in corresponding color as in Figure 4. Mutant residues in BA.1 RBD contributed interaction with S309 were shown in sphere. **B-C** The detailed interaction between H chain (**B**) or L chain (**C**) of S309 and the BA.1

RBD (**left panel**) or Prototype RBD (**right panel**). The residues involved in the interaction were labeled, and H-bonds were shown as dotted lines with a cutoff of 3.5 Å. **D** The overall comparison of two complex structures of S304/Prototype RBD and S304/BA.1 RBD by aligning the two RBDs. S304/Prototype RBD complex was shown in gray ribbon, and S304/BA.1 RBD is shown in corresponding color as in Figure 4. Mutant residues in BA.1 RBD contributed interaction with S304 were shown in sphere. **E-F** The detailed interaction between H chain (**E**) or L chain (**F**) of S304 and the BA.1 RBD (**left panel**) or Prototype RBD (**right panel**). The residues involved in the interaction were labeled, and H-bonds were shown as dotted lines with a cutoff of 3.5 Å. **G-I** Binding face between RBD and representative mAbs, including REGN10987 (**G**), S2A4 (**H**), and EY6A (**I**). All structures were shown in cartoon with the key residues in stick. H-bonds were shown as dotted lines with a cutoff of 3.5 Å. See also Tables S4-S6.

Figure 6. Binding characteristics of RBD-5 antibodies to Omicron BA.2 RBD with G446S mutation. The indicated antibodies were captured by a ProteinA chip. Then, serially diluted BA.2 RBD with G446S mutation were flowed over the chip surface to assess the binding, with BA.2 RBD for comparison. The raw and fitted curves are shown as dotted and solid lines, respectively. The K_D of each pair of interaction are shown as mean ± SD of three independent experiments. See also Figures S2 and S3.

STAR★METHODS

RESOURCE AVAILABILITY

Lead Contact

Further information and requests for resources and reagents should be directed to and will be fulfilled by the Lead Contact, George Fu Gao (gaof@im.ac.cn).

Materials Availability

All unique/stable reagents generated in this study are available from the Lead Contact with a completed Materials Transfer Agreement.

Data and Code Availability

Cryo-EM density map and atomic coordinates have been deposited in the Electron Microscopy Data Bank and Protein Data Bank with the accession codes EMD-32944 and 7X1M, respectively.

EXPERIMENTAL MODEL AND SUBJECT DETAILS

Cells

HEK293T cells (ATCC, CRL-3216) and Vero cells (ATCC, CCL81) were cultured at 37 ℃ in DMEM expression medium supplemented with 10% fetal bovine serum (FBS). HEK293F cells (Gibco, Cat# 11625-019) were cultured at 37 ℃ in SMM 293-TII expression medium (Sino Biological, Cat# M293TII) to express antibodies and RBDs.

METHOD DETAILS

Gene construction

The coding sequence of the variable region of each antibody was synthesized according to the amino acid sequences submitted to the Protein Data Bank. The heavy chains were fused with the constant region of human IgG1 and the light chains were fused with Igκ or Igλ, and both were cloned into the pCAGGS vector, respectively. The coding sequences of SARS-CoV-2 Prototype RBD (residues 319-541, GISAID:EPI_ISL_402119), Delta RBD (residues 319-541, GISAID:EPI_ISL_2020954), Omicron BA.1 RBD (residues 319-541, GISAID:EPI_ISL_6640916), Omicron BA.1.1 RBD (residues 319-541, GISAID:EPI_ISL_6704870), Omicron BA.2 RBD with or without G446S mutation

(residues 319-541, GISAID:EPI_ISL_9652748), and Omicron BA.3 RBD (residues 319-541, GISAID:EPI_ISL_7605589) with a C-terminal 6 × His tag were cloned into the pCAGGS vector, respectively. The SARS-CoV-2 Prototype S, Delta S, Omicron BA.1 S, Omicron BA.1.1 S, Omicron BA.2 S with or without G446S mutation, and Omicron BA.3 S with an 18 amino acid truncation at the C-terminus were constructed into the pCAGGS vectors for pseudovirus preparation, respectively.

Protein expression and purification

The heavy and light chain plasmids of each antibody were transiently co-transfected into HEK293T cells at a ratio of 2:3 using polyethylenimine. After 6 h, the supernatant of HEK293T cells was replaced with DMEM without FBS. The supernatant was collected three days post-transfection for SPR analysis. The heavy and light chain plasmids of each antibody were also transiently co-transfected into HEK293F cells to express antibodies for the pseudovirus assay. Five days later, the supernatant of HEK293F cells was collected and antibodies were purified using Protein A 5 mL affinity columns (GE Healthcare). RBD proteins were expressed in HEK293F cells and purified using HisTrap HP 5 mL affinity columns (GE Healthcare). The soluble proteins were further purified by gel filtration using a Superdex^{TM} 200 10/300 GL column (GE Healthcare). Fabs were generated by papain digestion and further purified using a Protein A column (S309 Fab and BD604 Fab) or Resourse Q column (S304 Fab) and gel filtration using a Superdex^{TM} 200 10/300 GL column. RBDs and Fabs for crystallization were stored in buffer containing 20 mM Tris-HCl and 150 mM NaCl (pH 8.0). Antibodies and RBDs for SPR analysis were stored in PBS.

SPR analysis

The binding affinities and kinetics between RBDs and mAbs were analyzed using the BIAcore 8K (GE Healthcare) at 25 ℃ in the single-cycle mode. PBST buffer (10 mM Na_2HPO_4, 2 mM KH_2PO_4, 137 mM NaCl, 2.7 mM KCl, pH 7.4, and 0.005% (v/v) Tween 20) was used as the running buffer, and RBD proteins were changed into this

buffer by gel filtration before use. First, culture supernatants containing the indicated antibodies were injected and captured on a Protein A chip (GE Healthcare). Serially diluted RBDs were then flowed over the surface of the chip to measure the binding response. Flow cell 1 was used as a negative control. 10 mM Glycine-HCl (pH 1.5) was used to regenerate the chips. The equilibrium dissociation constants (K_D) of each pair of interactions were calculated using a 1:1 (Langmuir) binding fit model with the BIAcore 8K evaluation software.

Pseudovirus neutralization assay

VSV-ΔG-GFP based SARS-CoV-2 prototype, Delta variant, Omicron BA.1, Omicron BA.1.1, Omicron BA.2 with or without G446S mutation and Omicron BA.3 pseudoviruses were prepared as previously described (Zheng et al., 2022). Briefly, 30 μg of the plasmids encoding spike protein was transfected into HEK 293T cells; 24 h later, the VSV-ΔG-G-GFP pseudoviruses were added there. After 1 h of incubation, the HEK293T cell culture medium was removed and replaced with fresh complete DMEM medium containing 10 μg/mL of anti-VSV-G antibody (I1-Hybridoma ATCC® CRL2700). After another 30 h, supernatants containing VSV-ΔG-GFP based pseudoviruses were harvested, centrifuged, and filtered through a 0.45 μm sterilized membrane filter. The pseudoviruses were then aliquoted and stored at -80 °C until use. For the neutralization assay, Vero cells were seeded in 96-well plates 12 h prior to infection. The antibodies were 4-fold serially diluted starting from 100 μg/mL. Then, 50 μL of the serially diluted antibodies were incubated with 50 μL of each pseudovirus at 1,000 transducing units at 37 °C for 1 h. The mixtures were then added to pre-plated Vero cells. After 15 h of incubation, transducing unit numbers were calculated using a CQ1 confocal image cytometer (Yokogawa).

Cryo-EM data collection

To prepare the cryo-EM sample, 4.0 μL of the BD-604/S309/S304/BA.1 RBD complex proteins at approximately 0.2 mg/mL was placed on the glow-discharged CryoMatrix

R1.2/1.3 300-mesh grids (product no. M024-Au300-R12/13, Zhenjiang Lehua Technology Co. Ltd., China) and blotted for 2 s under a blot force of 0 at 4 °C and 100% humidity. The grids were immediately plunge-frozen in liquid ethane using a Vitrobot Mark IV (Thermo Fisher Scientific) and then transferred to a 300 kV Titan Krios transmission electron microscope equipped with a Gatan K3 detector and GIF Quantum energy filter. EPU software (Thermo Fisher Scientific) was used for automatic data collection. Movies were collected at 105,000 × magnification, with a calibrated pixel size of 0.85 Å. The defocus range was between -1.0 μm and -2.0 μm. Each movie was dose-fractionated into 32 frames with a total dose of 60 e-/Å^2.

Image process and 3D reconstruction

The detailed data-processing workflow is illustrated in Supplementary Figure 3. A total of 8,354 super-resolution movies were collected and corrected for drift using MotionCor2(Zheng et al., 2017), and the contrast transfer function (CTF) parameters were determined using patch CTF estimation implemented in cryoSPARC v.3.3.1(Punjani et al., 2017). Blob particle picking, particle extraction, and 2D classification were performed on a subset of 583 micrographs. Good classes were selected and subjected to template picking, resulting in 6,930,593 particles. Junk particles were removed through multiple rounds of 2D classification, and a clean set of 1,444,508 particles was selected for the initial reconstruction and iterative heterogeneous refinement. A total of 553,923 particles were used for homogeneous refinement, yielding a 2.74 Å map. The structure model was built and refined using Phenix(Adams et al., 2010) and COOT(Emsley and Cowtan, 2004).

QUANTIFICATION AND STATISTICAL ANALYSIS

Binding analysis

K_D values of SPR experiments were obtained with BIAcore 8K Evaluation software (GE Healthcare), using a 1:1 binding model. The values indicate the mean ± SD of three independent experiments.

724 **Neutralization analysis**

725 IC_{50} values of neutralization experiments were obtained using GraphPad Prism 8
726 software. The values were one representative results of two independent experiments.
727

728 **SUPPLEMENTAL TABLE**

729 **Table S1 Characteristics of the antibodies tested in our study, Related to Figures**
730 **1 and 2.** The information of 50 human neutralizing antibodies targeting SARS-CoV-2
731 RBD were shown.
732

References

Adams, P.D., Afonine, P.V., Bunkoczi, G., Chen, V.B., Davis, I.W., Echols, N., Headd, J.J., Hung, L.W., Kapral, G.J., Grosse-Kunstleve, R.W., et al. (2010). PHENIX: a comprehensive Python-based system for macromolecular structure solution. Acta Crystallogr. D Biol. Crystallogr. *66*, 213-221. 10.1107/S0907444909052925.

Cao, Y., Su, B., Guo, X., Sun, W., Deng, Y., Bao, L., Zhu, Q., Zhang, X., Zheng, Y., Geng, C., et al. (2020). Potent Neutralizing Antibodies against SARS-CoV-2 Identified by High-Throughput Single-Cell Sequencing of Convalescent Patients' B Cells. Cell *182*, 73-84 e16. 10.1016/j.cell.2020.05.025.

Cui, Z., Liu, P., Wang, N., Wang, L., Fan, K., Zhu, Q., Wang, K., Chen, R., Feng, R., Jia, Z., et al. (2022). Structural and functional characterizations of infectivity and immune evasion of SARS-CoV-2 Omicron. Cell *185*, 1-12. 10.1016/j.cell.2022.01.019.

Dejnirattisai, W., Huo, J., Zhou, D., Zahradnik, J., Supasa, P., Liu, C., Duyvesteyn, H.M.E., Ginn, H.M., Mentzer, A.J., Tuekprakhon, A., et al. (2022). SARS-CoV-2 Omicron-B.1.1.529 leads to widespread escape from neutralizing antibody responses. Cell *185*, 467-484 e415. 10.1016/j.cell.2021.12.046.

Du, P., Gao, G.F., and Wang, Q. (2022). The mysterious origins of the Omicron variant of SARS-CoV-2. Innovation (N Y) *3*, 100206. 10.1016/j.xinn.2022.100206.

Emsley, P., and Cowtan, K. (2004). Coot: model-building tools for molecular graphics. Acta Crystallogr. D Biol. Crystallogr. *60*, 2126-2132. 10.1107/S0907444904019158.

Gobeil, S.M., Henderson, R., Stalls, V., Janowska, K., Huang, X., May, A., Speakman, M., Beaudoin, E., Manne, K., Li, D., et al. (2022). Structural diversity of the SARS-CoV-2 Omicron spike. bioRxiv. 10.1101/2022.01.25.477784.

Grabowski, F., Kochańczyk, M., and Lipniacki, T. (2022). The spread of SARS-CoV-2 variant Omicron with the doubling time of 2.0–3.3 days can be explained by immune evasion. medRxiv. 10.1101/2021.12.08.21267494.

Han, P., Li, L., Liu, S., Wang, Q., Zhang, D., Xu, Z., Han, P., Li, X., Peng, Q., Su, C., et al. (2022). Receptor binding and complex structures of human ACE2 to spike RBD from omicron and delta SARS-CoV-2. Cell *185*, 630-640 e610. 10.1016/j.cell.2022.01.001.

Hansen, C.H., Schelde, A.B., Moustsen-Helm, I.R., Emborg, H.-D., Krause, T.G., Mølbak, K., Valentiner-Branth, P., and Institut, o.b.o.t.I.D.P.G.a.S.S. (2021). Vaccine effectiveness against SARS-CoV-2 infection with the Omicron or Delta variants following a two-dose or booster BNT162b2 or mRNA-1273 vaccination series: A Danish cohort study. medRxiv. 10.1101/2021.12.20.21267966.

Harvey, W.T., Carabelli, A.M., Jackson, B., Gupta, R.K., Thomson, E.C., Harrison, E.M., Ludden, C., Reeve, R., Rambaut, A., Consortium, C.-G.U., et al. (2021). SARS-CoV-2 variants, spike mutations and immune escape. Nat. Rev. Microbiol. *19*, 409-424. 10.1038/s41579-021-00573-0.

Hastie, K.M., Li, H., Bedinger, D., Schendel, S.L., Dennison, S.M., Li, K., Rayaprolu, V., Yu, X., Mann, C., Zandonatti, M., et al. (2021). Defining variant-resistant epitopes targeted by SARS-CoV-2 antibodies: A global consortium study. Science *374*, 472-478. 10.1126/science.abh2315.

Hong, Q., Han, W., Li, J., Xu, S., Wang, Y., Li, Z., Wang, Y., Zhang, C., Huang, Z., and Cong, Y. (2022). Molecular basis of SARS-CoV-2 Omicron variant receptor engagement and antibody evasion and neutralization. bioRxiv. 10.1101/2022.01.10.475532.

Jiang, S., Shi, Z., Shu, Y., Song, J., Gao, G.F., Tan, W., and Guo, D. (2020). A distinct name is

needed for the new coronavirus. Lancet *395*, 949. 10.1016/S0140-6736(20)30419-0.
Karim, S.S.A., and Karim, Q.A. (2021). Omicron SARS-CoV-2 variant: a new chapter in the COVID-19 pandemic. Lancet *398*, 2126-2128. 10.1016/S0140-6736(21)02758-6.
Li, Q., Nie, J., Wu, J., Zhang, L., Ding, R., Wang, H., Zhang, Y., Li, T., Liu, S., Zhang, M., et al. (2021). SARS-CoV-2 501Y.V2 variants lack higher infectivity but do have immune escape. Cell *184*, 2362-2371 e2369. 10.1016/j.cell.2021.02.042.
Li, Z., Li, S., Zhang, G., Peng, W., Chang, Z., Zhang, X., Fan, Z., Chai, Y., Wang, F., Zhao, X., et al. (2022). An engineered bispecific human monoclonal antibody against SARS-CoV-2. Nat. Immunol. *23*, 423-430. 10.1038/s41590-022-01138-w.
Liu, C., Ginn, H.M., Dejnirattisai, W., Supasa, P., Wang, B., Tuekprakhon, A., Nutalai, R., Zhou, D., Mentzer, A.J., Zhao, Y., et al. (2021a). Reduced neutralization of SARS-CoV-2 B.1.617 by vaccine and convalescent serum. Cell *184*, 4220-4236 e4213. 10.1016/j.cell.2021.06.020.
Liu, L., Iketani, S., Guo, Y., Chan, J.F., Wang, M., Liu, L., Luo, Y., Chu, H., Huang, Y., Nair, M.S., et al. (2021b). Striking antibody evasion manifested by the Omicron variant of SARS-CoV-2. Nature *602*, 676-681. 10.1038/s41586-021-04388-0.
Lopez Bernal, J., Andrews, N., Gower, C., Gallagher, E., Simmons, R., Thelwall, S., Stowe, J., Tessier, E., Groves, N., Dabrera, G., et al. (2021). Effectiveness of Covid-19 Vaccines against the B.1.617.2 (Delta) Variant. N Engl J Med *385*, 585-594. 10.1056/NEJMoa2108891.
Piccoli, L., Park, Y.J., Tortorici, M.A., Czudnochowski, N., Walls, A.C., Beltramello, M., Silacci-Fregni, C., Pinto, D., Rosen, L.E., Bowen, J.E., et al. (2020). Mapping Neutralizing and Immunodominant Sites on the SARS-CoV-2 Spike Receptor-Binding Domain by Structure-Guided High-Resolution Serology. Cell *183*, 1024-1042 e1021. 10.1016/j.cell.2020.09.037.
Pinto, D., Park, Y.J., Beltramello, M., Walls, A.C., Tortorici, M.A., Bianchi, S., Jaconi, S., Culap, K., Zatta, F., De Marco, A., et al. (2020). Cross-neutralization of SARS-CoV-2 by a human monoclonal SARS-CoV antibody. Nature *583*, 290-295. 10.1038/s41586-020-2349-y.
Planas, D., Saunders, N., Maes, P., Guivel-Benhassine, F., Planchais, C., Buchrieser, J., Bolland, W.H., Porrot, F., Staropoli, I., Lemoine, F., et al. (2021a). Considerable escape of SARS-CoV-2 Omicron to antibody neutralization. Nature *602*, 671-675. 10.1038/s41586-021-04389-z.
Planas, D., Veyer, D., Baidaliuk, A., Staropoli, I., Guivel-Benhassine, F., Rajah, M.M., Planchais, C., Porrot, F., Robillard, N., Puech, J., et al. (2021b). Reduced sensitivity of SARS-CoV-2 variant Delta to antibody neutralization. Nature *596*, 276-280. 10.1038/s41586-021-03777-9.
Punjani, A., Rubinstein, J.L., Fleet, D.J., and Brubaker, M.A. (2017). cryoSPARC: algorithms for rapid unsupervised cryo-EM structure determination. Nat. Methods *14*, 290-296. 10.1038/nmeth.4169.
Shi, R., Shan, C., Duan, X., Chen, Z., Liu, P., Song, J., Song, T., Bi, X., Han, C., Wu, L., et al. (2020). A human neutralizing antibody targets the receptor-binding site of SARS-CoV-2. Nature *584*, 120-124. 10.1038/s41586-020-2381-y.
Tan, W., Zhao, X., Ma, X., Wang, W., Niu, P., Xu, W., Gao, G.F., and Wu, G. (2020). A Novel Coronavirus Genome Identified in a Cluster of Pneumonia Cases - Wuhan, China 2019-2020. China CDC Wkly *2*, 61-62.
Tseng, H.F., Ackerson, B.K., Luo, Y., Sy, L.S., Talarico, C.A., Tian, Y., Bruxvoort, K.J., Tubert, J.E., Florea, A., Ku, J.H., et al. (2022). Effectiveness of mRNA-1273 against SARS-CoV-2 Omicron and Delta variants. Nat. Med. *28*, 1063-1071. 10.1038/s41591-022-01753-y.
VanBlargan, L.A., Errico, J.M., Halfmann, P.J., Zost, S.J., Crowe, J.E., Jr., Purcell, L.A., Kawaoka, Y.,

Corti, D., Fremont, D.H., and Diamond, M.S. (2022). An infectious SARS-CoV-2 B.1.1.529 Omicron virus escapes neutralization by therapeutic monoclonal antibodies. Nat. Med. *28*, 490-495. 10.21203/rs.3.rs-1175516/v1.

Wang, Q., Zhang, Y., Wu, L., Niu, S., Song, C., Zhang, Z., Lu, G., Qiao, C., Hu, Y., Yuen, K.Y., et al. (2020). Structural and Functional Basis of SARS-CoV-2 Entry by Using Human ACE2. Cell *181*, 894-904 e899. 10.1016/j.cell.2020.03.045.

WHO (2021a). Classification of Omicron (B.1.1.529): SARS-CoV-2 Variant of Concern. https://www.who.int/news/item/26-11-2021-classification-of-omicron-(b.1.1.529)-sars-cov-2-variant-of-concern.

WHO (2021b). Enhancing readiness for Omicron (B.1.1.529): technical brief and priority actions for member states (WHO - 17 December 2021. https://www.who.int/publications/m/item/enhancing-readiness-for-omicron-(b.1.1.529)-technical-brief-and-priority-actions-for-member-states.

WHO (2022). Weekly epidemiological update on COVID-19 - 22 March 2022. https://www.who.int/publications/m/item/weekly-epidemiological-update-on-covid-19---22-march-2022.

Wu, Y., Wang, F., Shen, C., Peng, W., Li, D., Zhao, C., Li, Z., Li, S., Bi, Y., Yang, Y., et al. (2020). A noncompeting pair of human neutralizing antibodies block COVID-19 virus binding to its receptor ACE2. Science *368*, 1274-1278. 10.1126/science.abc2241.

Yuan, M., Liu, H., Wu, N.C., Lee, C.D., Zhu, X., Zhao, F., Huang, D., Yu, W., Hua, Y., Tien, H., et al. (2020a). Structural basis of a shared antibody response to SARS-CoV-2. Science *369*, 1119-1123. 10.1126/science.abd2321.

Yuan, M., Wu, N.C., Zhu, X., Lee, C.D., So, R.T.Y., Lv, H., Mok, C.K.P., and Wilson, I.A. (2020b). A highly conserved cryptic epitope in the receptor binding domains of SARS-CoV-2 and SARS-CoV. Science *368*, 630-633. 10.1126/science.abb7269.

Zhao, X., Li, D., Ruan, W., Chen, Z., Zhang, R., Zheng, A., Qiao, S., Zheng, X., Zhao, Y., Dai, L., et al. (2022). Effects of a Prolonged Booster Interval on Neutralization of Omicron Variant. N Engl J Med *386*, 894-896. 10.1056/NEJMc2119426.

Zheng, A., Wu, L., Ma, R., Han, P., Huang, B., Qiao, C., Wang, Q., Tan, W., Gao, G.F., and Han, P. (2022). A binding-enhanced but enzymatic activity-eliminated human ACE2 efficiently neutralizes SARS-CoV-2 variants. Signal Transduct Target Ther *7*, 10. 10.1038/s41392-021-00821-y.

Zheng, S.Q., Palovcak, E., Armache, J.P., Verba, K.A., Cheng, Y., and Agard, D.A. (2017). MotionCor2: anisotropic correction of beam-induced motion for improved cryo-electron microscopy. Nat. Methods *14*, 331-332. 10.1038/nmeth.4193.

Zhou, D., Dejnirattisai, W., Supasa, P., Liu, C., Mentzer, A.J., Ginn, H.M., Zhao, Y., Duyvesteyn, H.M.E., Tuekprakhon, A., Nutalai, R., et al. (2021). Evidence of escape of SARS-CoV-2 variant B.1.351 from natural and vaccine-induced sera. Cell *184*, 2348-2361 e2346. 10.1016/j.cell.2021.02.037.

Zhu, N., Zhang, D., Wang, W., Li, X., Yang, B., Song, J., Zhao, X., Huang, B., Shi, W., Lu, R., et al. (2020). A Novel Coronavirus from Patients with Pneumonia in China, 2019. N Engl J Med *382*, 727-733. 10.1056/NEJMoa2001017.

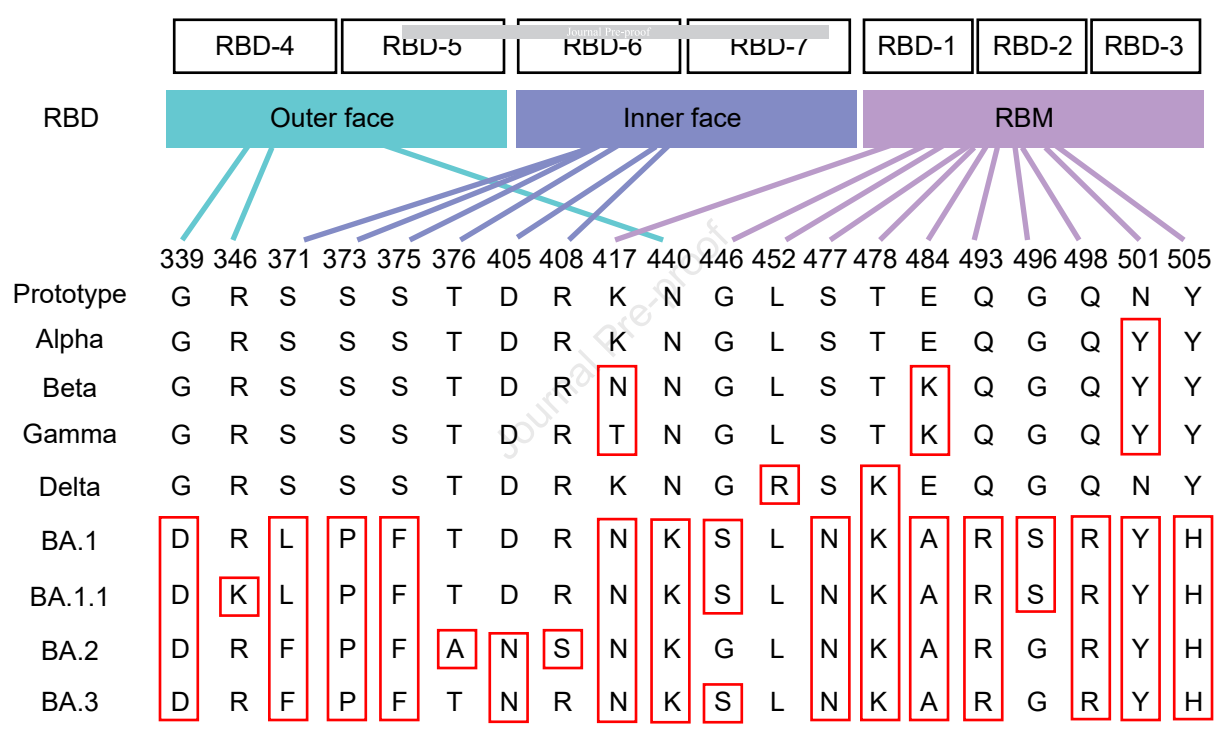

Class	Ab	Binding affinity (K_D: nM)						Pseudovirus neutralization (IC_{50}: μg/ml)						
		BA.1	BA.1.1	BA.2	BA.3	Delta	PT	BA.1	BA.1.1	BA.2	G446S	BA.3	Delta	PT
RBD-1	CB6	-	-	-	871.4	13.3	27.2	>100	>100	>100	>100	>100	0.008	0.02
	B38	-	-	3500	535.6	94.6	226.1	>100	>100	>100	>100	>100	0.059	1.76
	BD-236	-	-	-	2094	2.5	7.8	>100	>100	>100	>100	>100	0.038	0.065
	BD-604	6.1	14.7	11.1	2.0	0.002	0.05	0.17	0.049	0.1	0.066	0.013	0.023	0.027
	BD-629	19.2	26.6	97.1	58.0	0.1	0.8	0.78	1.356	0.98	2.5	1.08	0.014	0.03
	C102	235.8	1061	456.4	432.2	19.6	49.0	>100	>100	>100	>100	>100	0.02	0.067
	C105	-	-	-	2460	9.3	17.4	>100	>100	>100	>100	>100	0.034	0.15
	C1A-B3	-	-	-	-	20.1	41.9	>100	>100	>100	>100	>100	0.01	0.03
	C1A-C2	-	-	-	-	7.4	17.2	>100	>100	>100	>100	>100	0.01	0.021
	C1A-F10	-	-	-	-	5.7	16.8	>100	>100	>100	>100	>100	0.018	0.017
	CC12.1	203.9	451.3	584.9	880.2	10.4	23.3	>100	>100	>100	>100	>100	0.012	0.007
	CC12.3	181.4	412.0	180.3	363.8	6.6	13.5	16.54	5.42	20.54	18.56	23.7	0.003	0.003
	COVA2-04	-	-	-	-	26.8	55.5	>100	>100	>100	>100	>100	0.23	1.23
	CV30	160.1	778	668.1	1038	4.2	8.4	>100	>100	>100	>100	>100	0.013	0.046
	P2C-1F11	41.8	70.8	61.5	39.8	3.1	6.3	3.81	2.62	0.53	1.04	2.57	0.012	0.039
	S2H14	-	-	-	-	56.1	135.5	>100	>100	>100	>100	>100	0.46	5.39
RBD-2	REGN10933	11.9	40.6	41.6	104.6	0.3	1.9	>100	>100	>100	>100	>100	0.005	0.011
	LY-CoV555	-	-	-	-	60.7	2.7	>100	>100	>100	>100	>100	2.89	0.01
	Ab23	-	-	-	-	920.9	734.7	>100	>100	>100	>100	>100	0.45	0.86
	COVA2-39	4145	5783	2156	3242	26.3	23.5	>100	>100	>100	>100	>100	0.14	0.18
	C121	-	-	-	-	34.8	7.5	>100	>100	>100	>100	>100	0.32	0.003
	C144	-	-	-	-	34.7	118.6	>100	>100	>100	>100	>100	0.01	0.009
	P2C-1A3	-	-	-	-	57.3	128.7	>100	>100	>100	>100	>100	4.09	2.28
	H4	3577	-	-	-	24.6	18.5	>100	>100	>100	>100	>100	0.027	0.49
	S2E12	44.0	114.0	80.2	103.1	2.0	2.1	0.61	0.16	0.66	0.047	2.43	0.001	0.003
	S2M11	-	-	-	-	32.0	82.5	>100	>100	>100	>100	>100	0.003	0.004
	2-4	-	-	-	-	22.6	57.0	>100	>100	>100	>100	>100	0.11	0.61
RBD-3	ADI-56046	2342	1453	-	18033	0.3	0.3	>100	>100	>100	>100	>100	0.036	0.087
RBD-4	BD-368-2	2053	4700	4781	2464	309.5	10.6	>100	>100	>100	>100	>100	>100	0.003
	C002	-	-	-	-	68	74.4	>100	>100	>100	>100	>100	15.78	0.12
	C104	-	-	-	-	87.5	67.7	>100	>100	>100	>100	>100	27.26	0.19
	CV07-270	2152	-	201.8	963.8	2626	18.7	>100	>100	>100	>100	>100	>100	0.029
	P17	-	-	-	3456	17.4	15.7	>100	>100	>100	>100	>100	0.006	0.007
	P2B-2F6	-	-	5140	-	16.7	96.8	>100	>100	>100	>100	>100	7.36	0.021
	S2H13	-	-	-	-	62.2	256.0	>100	>100	>100	>100	>100	0.522	2.57
RBD-5	REGN10987	3570	9290	56.7	3031	11.3	20.5	>100	>100	0.45	>100	>100	0.006	0.006
	C110	329.6	382.7	242.4	405.2	71.4	2.4	>100	>100	18.54	>100	>100	0.81	0.012
	C119	-	-	4583	-	2.2	10.8	>100	>100	>100	>100	>100	0.003	0.011
	C135	-	-	-	-	1.3	5.0	>100	>100	>100	>100	>100	0.003	0.007
	S309	0.9	0.7	4.2	2.6	0.09	0.3	0.085	0.086	0.19	0.27	0.015	0.016	0.021
	2H04	354.0	-	2109	1452	185.5	133.5	>100	>100	6.01	>100	>100	3.97	3.04
	47D11	-	-	-	-	88.0	114.4	>100	>100	>100	>100	>100	0.45	0.33
RBD-6	COVA1-16	35.0	80.2	70.6	60.9	26.9	39.3	6.91	7.12	21.8	44.89	>100	0.087	0.6
	C022	6.5	2.6	8.5	3.1	2.3	4.4	8.16	9.0	21.64	5.67	33.6	0.35	0.27
	2-36	52.4	29.4	37.8	36.6	12.1	25.5	40.37	13.94	>100	>100	>100	0.15	0.12
RBD-7	CR3022	12.1	16.3	33.5	9.8	12.1	19.2	>100	>100	>100	>100	>100	>100	>100
	EY6A	3.2	2.2	3.3	1.7	10.2	11.5	1.06	0.85	0.32	0.24	0.078	0.35	0.22
	H014	657.9	1105	1342	642.0	0.8	0.4	>100	>100	>100	>100	>100	0.9	0.98
	S2A4	986.7	1116	68.1	67.5	2.8	9.0	>100	>100	>100	>100	>100	0.58	2.96
	S304	2.6	1.2	2.6	0.7	1.2	4.4	>100	>100	>100	>100	>100	2.28	13.26

-	not determined	>1000	10-1000	1-10	<1	>100	10-100	1-10	0.1-1	<0.1

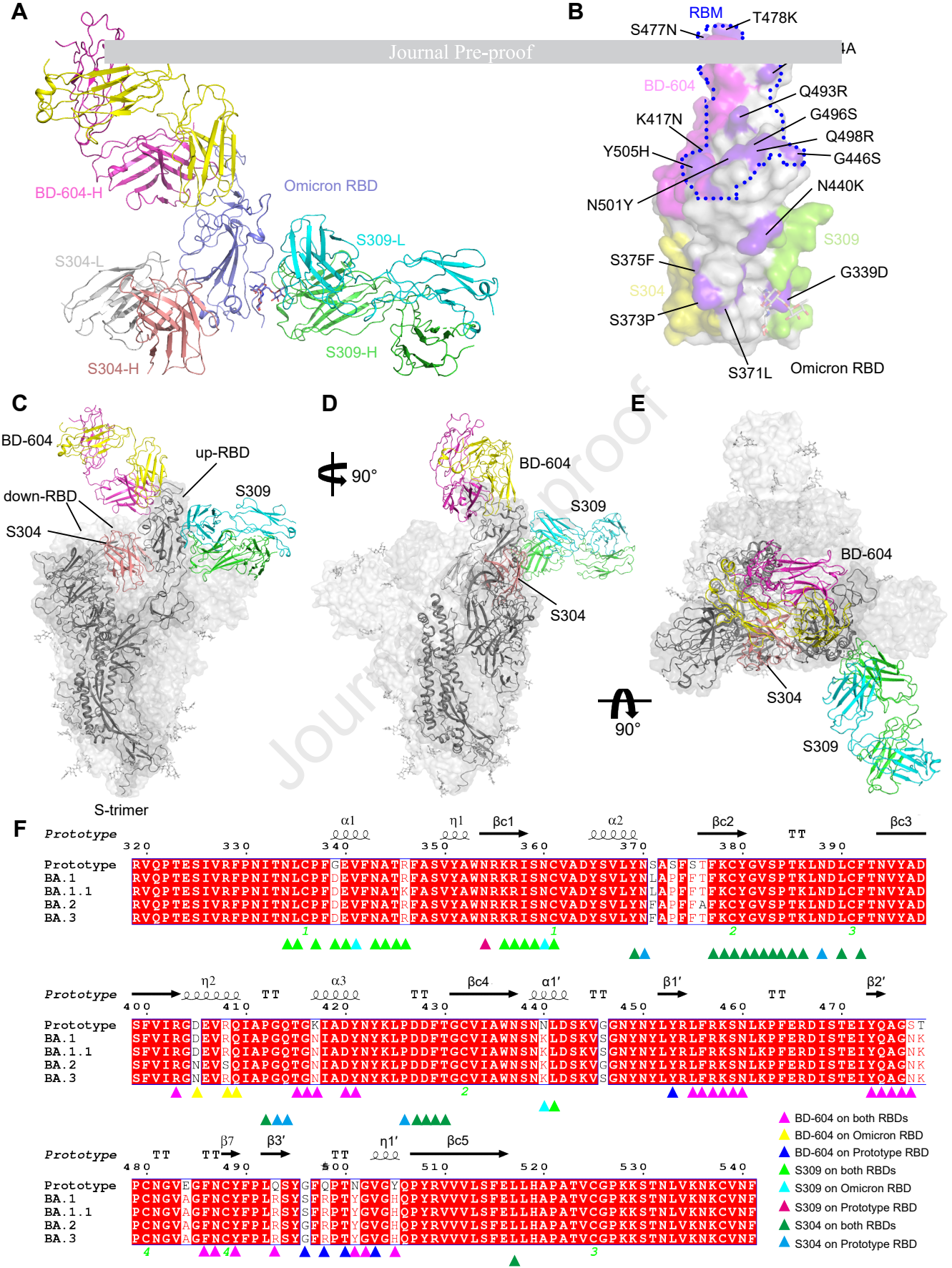

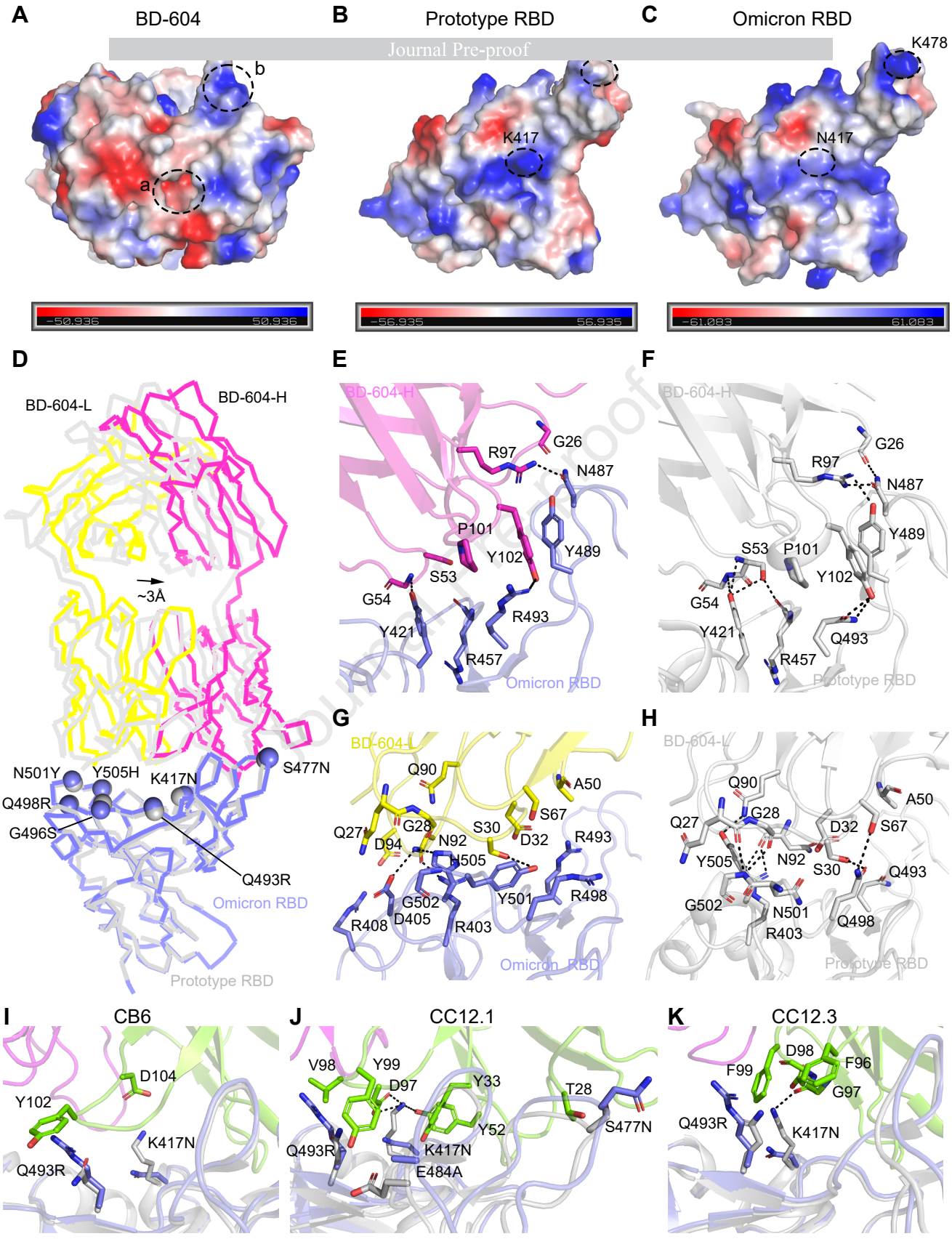

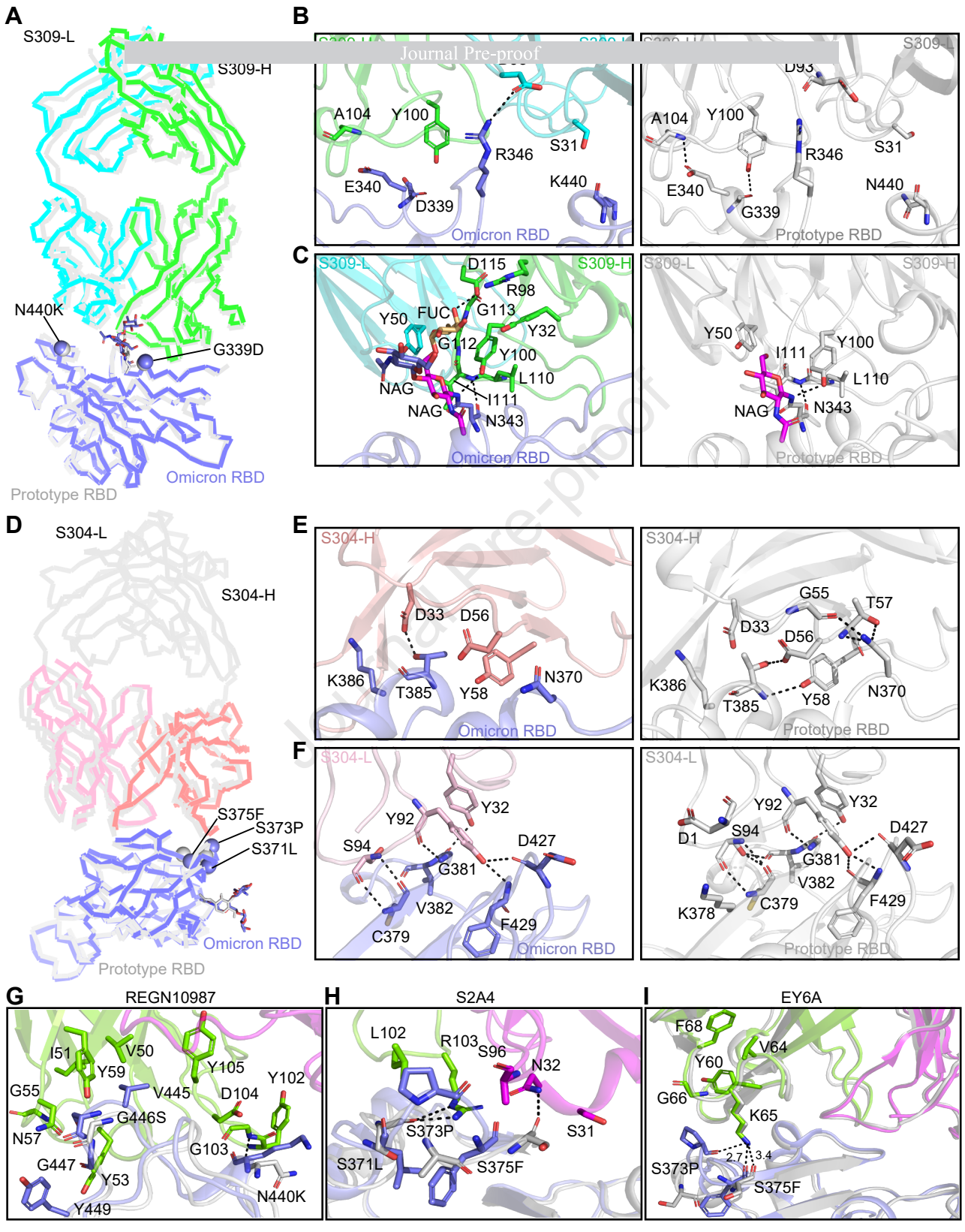

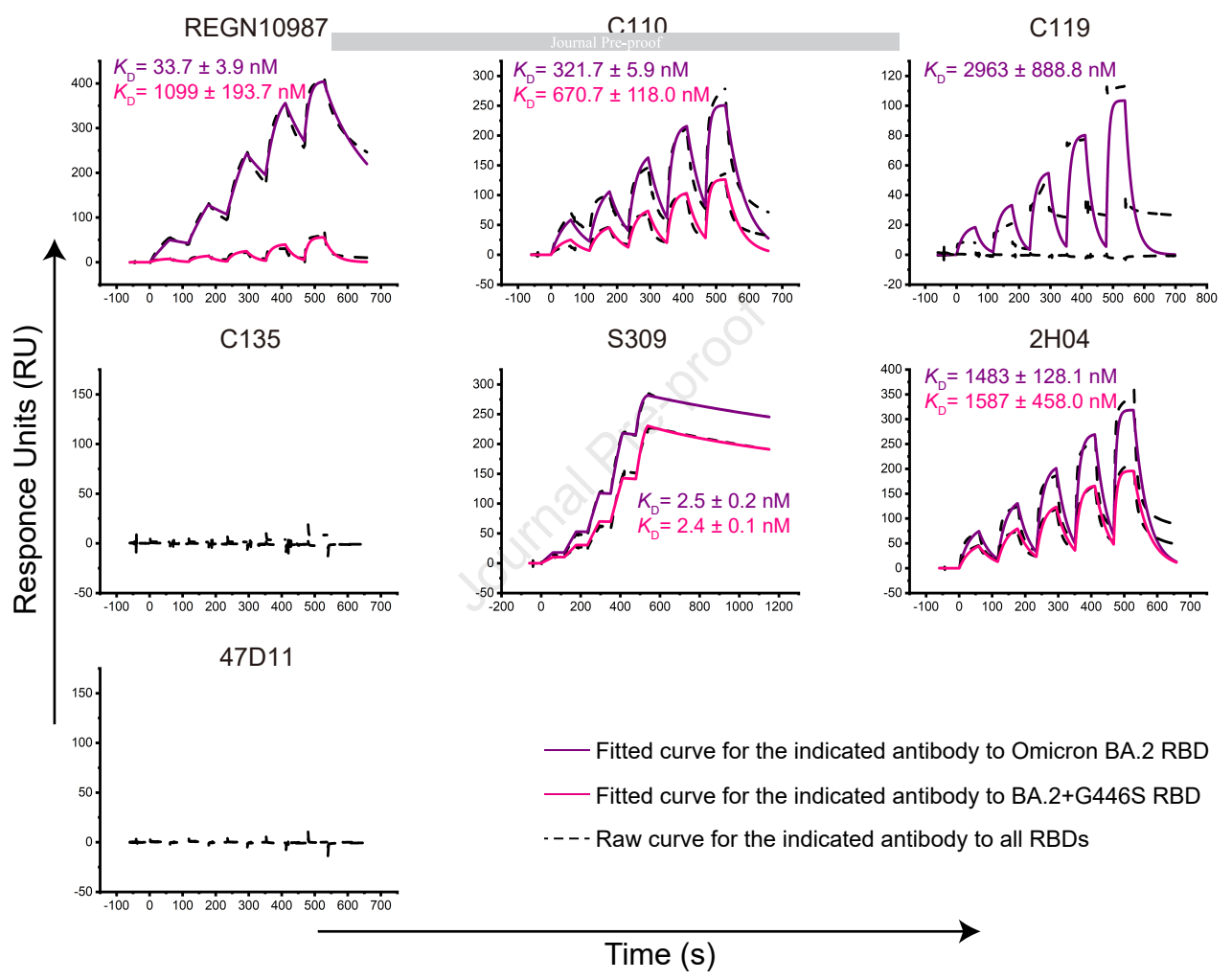

Highlights

Immune escape of 50 human mAbs by Omicron sub-variants was assessed.

Omicron BA.1, BA.1.1, BA.2 and BA.3 have similar immune evasion spectra.

BA.2 is more sensitive to RDB-5 mAbs due to the lack of G446S mutation.

eTOC Blurb

The evolution of SARS-CoV-2 variants of concern brings new challenges toward host immunity and protection. Huang et al. tested the neutralization potency of 50 human mAbs against Omicron sub-variants BA.1, BA.1.1, BA.2 and BA.3. Structural analysis of three mAbs provides further insight into the immune evasion capacity of Omicron sub-variants.

KEY RESOURCES TABLE

REAGENT or RESOURCE	SOURCE	IDENTIFIER
Bacterial Strains		
Escherichia coli (E. coli) strain DH5α	Vazyme	Cat# C502-02
Chemicals, antibody, and Recombinant Proteins		
Polyethylenimine (PEI)	Polysciences	Cat# 24885-2
L-Cysteine •HCl•H_2O	Thermo scientific	Cat#44889
Immobilized Papain	Thermo scientific	Cat#20341
anti-VSV-G antibody	I1-Hybridoma ATCC®	Cat#CRL2700
SARS-CoV-2 Prototype RBD protein with His-tag, spike residues 319-541	This paper	GISAID:EPI_ISL_ 402119
SARS-CoV-2 Delta RBD protein with His-tag, spike residues 319-541	This paper	GISAID:EPI_ISL_2020954
SARS-CoV-2 Omicron BA.1 RBD protein with His-tag, spike residues 319-541	This paper	GISAID:EPI_ISL_6640916
SARS-CoV-2 Omicron BA.1.1 RBD protein with His-tag, spike residues 319-541	This paper	GISAID:EPI ISL_6704870
SARS-CoV-2 Omicron BA.2 RBD protein with His-tag, spike residues 319-541	This paper	GISAID:EPI_ISL_9652748
SARS-CoV-2 Omicron BA.2 RBD with G446S mutation protein with His-tag, spike residues 319-541	This paper	GISAID:EPI_ISL_9652748
SARS-CoV-2 Omicron BA.3 RBD protein with His-tag, spike residues 319-541	This paper	GISAID:EPI_ISL_7605589
Critical Commercial Assays		
HisTrap HP 5 mL column	GE Healthcare	Cat# 17524802
Protein A HP 5 mL column	GE Healthcare	Cat#17040303
HiLoad 16/600 Superdex 200 pg	GE Healthcare	Cat# 28989335
Membrane concentrator	Millipore	UFC901096
Series S Sensor Chip Protein A	GE Healthcare	Cat#29127556
Deposited Data		
BD-604 Fab/S304 Fab/S309 Fab/Omicron BA.1 RBD (Cryo-EM)	This paper	Protein Data Bank: 7X1M
Experimental Models: Cell Lines		

HEK293T cells	ATCC	ATCC CRL-3216
HEK293F cells	Gibco	Cat# 11625-019
Vero cells	ATCC	ATCC CCL-81
Recombinant DNA		
pCAGGS	MiaoLingPlasmid	Cat# P0165
pCAGGS-mAbs	This paper	Sequence from PDB in Table S1
pCAGGS-VSV-ΔG-GFP	This paper	N/A
pCAGGS-SARS-CoV-2 Prototype S	This paper	GISAID:EPI_ISL_ 402119
pCAGGS-SARS-CoV-2 Delta S	This paper	GISAID:EPI_ISL_2020954
pCAGGS-SARS-CoV-2 Omicron BA.1 S	This paper	GISAID:EPI_ISL_6640916
pCAGGS-SARS-CoV-2 Omicron BA.1.1 S	This paper	GISAID:EPI ISL_6704870
pCAGGS-SARS-CoV-2 Omicron BA.2 S	This paper	GISAID:EPI_ISL_9652748
pCAGGS-SARS-CoV-2 Omicron BA.2 S with G446S mutation	This paper	GISAID:EPI_ISL_9652748
pCAGGS-SARS-CoV-2 Omicron BA.3 S	This paper	GISAID:EPI_ISL_7605589
Software and Algorithms		
PyMOL software	Molecular Graphics System, Version 1.8 Schrö dinger	https://pymol.org /2/
BIAcore® 8K Evaluation software	GE Healthcare	N/A
Motioncor2	(Zheng et al., 2017)	N/A
COOT	(Emsley and Cowtan, 2004)	http://www.mrc-lmb.cam.ac.uk/personal/peemsley/coot/
Phenix	(Adams et al., 2010)	http://www.phenix-online.org/
MolProbity	Duke Biochemistry	http://molprobity.biochem.duke.edu/index.php